Incompressible Rayleigh-Taylor Turbulence

Rayleigh-Taylor turbulence

Guido Boffetta[1] and Andrea Mazzino[2]

[1]Department of Physics and INFN, University of Torino, Italy; email: guido.boffetta@unito.it
[2]Department of Civil, Chemical and Environmental Engineering, INFN and CINFAI, University of Genova, Italy; email: andrea.mazzino@unige.it

Xxxx. Xxx. Xxx. Xxx. YYYY. AA:1–27

This article's doi:
10.1146/((please add article doi))

Keywords

Turbulent convection, Mixing, Heat and mass transfer, Complex flows

Abstract

Basic fluid equations are the main ingredient to develop theories of the Rayleigh–Taylor buoyancy-induced instability. Turbulence arises in the late stage of the instability evolution as a result of the proliferation of active scales of motion. Fluctuations are maintained by the unceasing conversion of potential energy into kinetic energy. Although the dynamics of turbulent fluctuations is ruled by the same equations controlling the Rayleigh–Taylor instability, here only phenomenological theories are currently available. The main purpose of the present review is to provide an overview of the most relevant (and often contrasting) theoretical approaches to Rayleigh–Taylor turbulence together with numerical and experimental evidences for their support. Although the focus will be mainly on the classical Boussinesq Rayleigh–Taylor turbulence of miscible fluids, the review extends to other fluid systems having viscoelastic behavior, being affect by rotation of the reference frame and, finally, in the presence of reactions.

1. INTRODUCTION

The Rayleigh-Taylor (RT) instability arises at the interface of two fluids of different densities in presence of relative acceleration. The RT instability, and its late-stage evolution in a fully developed turbulent regime, are ubiquitous spontaneous mixing phenomena occurring in many natural systems having unstably stratified interfaces. They also occur over a huge interval of spatial and temporal scales, ranging from everyday-life phenomena to astrophysical processes.

In astrophysics, the RT instability is thought to have profound consequences for flame acceleration in type Ia supernova. It is possible that this acceleration, operating on the stellar scale, can bring the flame speed up to a significant fraction of the speed of sound, a fact with important consequences in modeling Type Ia supernovae (see, e.g., Hillebrandt & Niemeyer (2000) and Bell et al. (2004)). In geology, multi-wavelength RT instability has been invoked to explain the initiation and evolution of Polydiapirs (domes-in-domes) (see, e.g., Weinberg & Schmeling (1992)). Moreover, the possibility that intraplate orogeny is the result of RT instability of the Earth's mantle lithosphere beneath the orogenic zone has been explored by means of a two-layered model (Neil & Houseman 1999). In atmospheric fluid dynamics and cloud physics, RT instability has been called into play by Agee (1975) to try to solve the intriguing enigma related to the mechanism of formation of the fascinating mammatus clouds. As discussed by Shultz et al. (2006), the situation is however still rather controversial and further investigations are needed.

RT instability and turbulence also have a key role in several technological applications as, by way of example, the inertial confinement fusion and the disruption of radio-wave propagation within the terrestrial ionosphere. In the inertial confinement fusion, the RT instability causes a premature fuel mixing (due to beam-beam imbalance and/or beam anisotropy) thus reducing heating efficacy at the time of maximum compression (see, e.g., Tabak et al. (1994); Kilkenny et al. (1994)). In the terrestrial ionosphere, electromagnetic waves are scattered due to irregularities in plasma density. RT instability is invoked to explain these irregularities (see, e.g., Sultan (1996)).

Even if in all discussed cases the basic mechanism of RT instability and turbulence is a buoyancy induced fluid-mixing mechanism, many other ingredients may actually enter into play. We cite surface tension and viscosity (see, e.g., Bellman & Pennington (1954); Mikaelian (1993); Chertkov et al. (2005); Celani et al. (2009); Boffetta et al. (2010c)), magnetic fields (Kruskal & Schwarzschild 1954; Peterson et al. 1996), spherical geometries (Plesset 1954; Sakagami & Nishihara 1990), finite-amplitude perturbations (Chang 1959), bubbles (Garabedian 1957; Hecht et al. 1994; Goncharov 2002), rotation (Chandrasekhar 1961; Baldwin et al. 2015), and compressibility (Newcomb 1983; Scagliarini et al. 2010).

The field of RT instability appears to be very mature and there exist already excellent reviews of parts of the instability theory, especially those by Chandrasekhar (1961) and, more recently, by Sharp (1984) and by Abarzhi (2010b). Chandrasekhar's work gives an overview on the linear theory for incompressible continuous media, while Sharp surveys also nonlinear phenomenological models. Abarzhi (2010b) extends the review to include the nonlinear mixing stage. The textbook of Drazin & Reid (1981) represents another valuable introduction to hydro-dynamic instabilities. Thermal instabilities and shear flow instabilities are the main concern of the excellent review by Kull (1991). The review by Andrews & Dalziel (2010) reports the recent progresses in the experiments on RT mixing at low Atwood numbers.

Our aim here is to try to summarize about one decade of research activity on the

phenomenology of (miscible) Boussinesq RT turbulence after the seminal paper by Chertkov (2003). This paper deeply changed the way to think about Boussinesq RT turbulence: it now appears as a classical hydrodynamical turbulence system where the role of gravity is simply to act as a time-dependent pumping scale. Familiar concepts borrowed from the classical theory, *à la* Kolmogorov, of turbulent flows have thus been exploited for the Boussinesq RT system with many predictions for relevant statistical observables. These predictions triggered new studies with the final aim to confirm or contradict the new theory. One of the main aim of our review is to summarize the current state of the art in this respect. Moreover, we aim at providing a guided tour on generalizations of classical Boussinesq RT turbulence, including viscoelastic RT turbulence and RT mixing under rotation, with the hope they could trigger new experimental activities in this fields as well as make an interesting comparisons and connections with Rayleigh-Bénard turbulent system. Due to space constraints, we will not review many interesting and important aspects of RT mixing dealing with non-Boussinesq effects, immiscibility, compressibility and complex geometry.

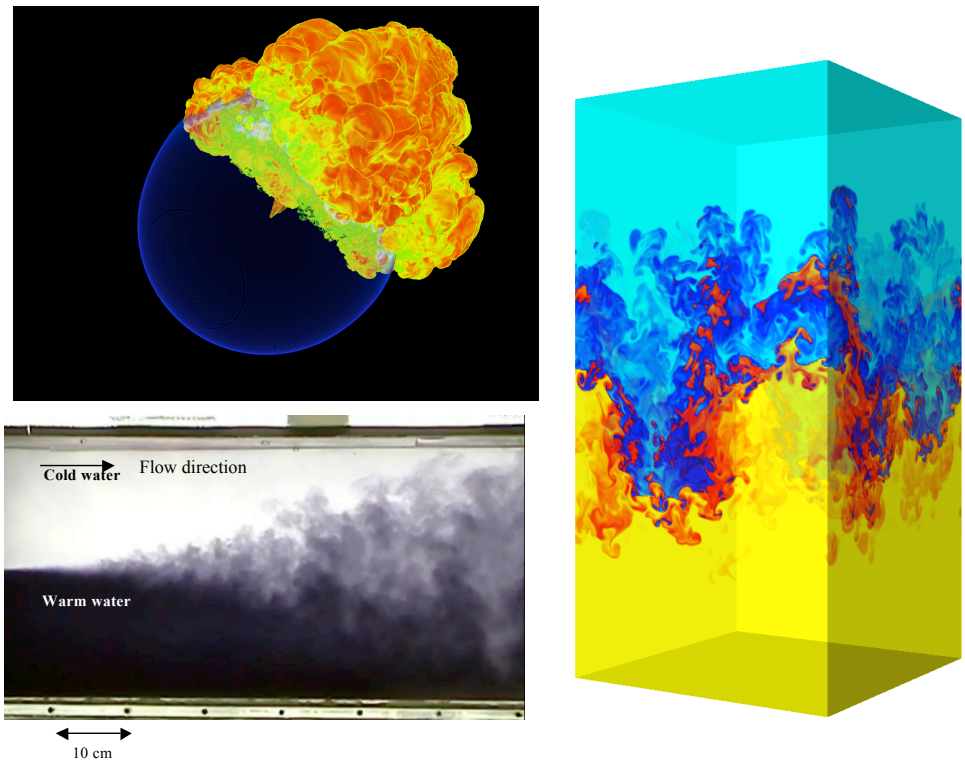

Figure 1

(Left upper) Thermonuclear flame plume bursting through the surface of a white dwarf during in supernova explosion (Image credit: Flash Center for Computational Science, University of Chicago). (Left lower) Rayleigh-Taylor mixing experiment in water channel: upper, clear, heavy water mixes by RT instability with lower, dark, light water generating turbulent mixing (Image courtesy of A. Banerjee). (Right) Color representation of the temperature field $T(\mathbf{x})$ (yellow=hot, blue=cold) from a Direct Numerical Simulation of the Boussinesq equations (2-3) in the late stage of RT turbulence.

2. Oberbeck-Boussinesq equations for Rayleigh-Taylor turbulence

One important application of RT instability is the case of convective flow, in which density differences reflect temperature fluctuations of a single fluid and the acceleration is provided by gravity, which is uniform in space. The problem is further simplified within the so-called Oberbeck-Boussinesq (OB) approximation (see, e.g., Tritton (1988)) which assumes incompressible flows and small variations of the density. In this limit, density ρ linearly depends on the temperature T as

$$\rho(T) = \rho(T_0)\left[1 - \beta(T - T_0)\right] \tag{1}$$

where T_0 is a reference temperature and the thermal expansion coefficient β (as well as the viscosity ν and the thermal diffusivity κ) is assumed constant, independent of T. The OB equations of motion for the velocity $\mathbf{u}(\mathbf{x}, t)$ and temperature $T(\mathbf{x}, t)$ in the gravitational field $\mathbf{g} = (0, 0, -g)$ are

$$\partial_t \mathbf{u} + \mathbf{u} \cdot \nabla \mathbf{u} = -\nabla p + \nu \nabla^2 \mathbf{u} - \beta \mathbf{g} T \tag{2}$$

$$\partial_t T + \mathbf{u} \cdot \nabla T = \kappa \nabla^2 T \tag{3}$$

together with the incompressibility condition $\nabla \cdot \mathbf{u} = 0$. We remark that under the OB approximation, the fluid motion is symmetric for vertical reflection: indeed equations (2-3) are invariant for $\mathbf{g} \to -\mathbf{g}$ and $T \to -T$. Rayleigh-Taylor configuration is defined by the initial condition of an unstable stratification with a horizontal interface (in general normal to the acceleration) which separates a layer of cooler (heavier, of density ρ_2) fluid from a lower layer of hotter (lighter, of density ρ_1) fluid, both at rest, i.e. $T(\mathbf{x}, 0) = -(\theta_0/2) sgn(z)$ and $\mathbf{u}(\mathbf{x}, 0) = 0$. θ_0 is the temperature jump across the layers (symmetric with respect to T_0) which fixes the Atwood number $A = (\rho_2 - \rho_1)/(\rho_2 + \rho_1) = \beta\theta_0/2$. Although the Atwood number must be small for the validity of the OB limit, when working within this approximation A simply rescales the effect of gravity on the buoyancy force and thus the characteristic time of the phenomena. In the rest of this Review we will always assume the validity of the OB approximation and therefore we will use the notion of either density fluctuation or temperature fluctuation as the two are related by (1).

The RT configuration is unstable to perturbations of the interface. We remark that in numerical and experimental applications it is sometime useful to introduce some smoothing of the interface over a finite thickness. For a single mode perturbation of wavenumber k, linear stability analysis for an inviscid potential flow gives the growth rate of the amplitude as (see Lamb (1932) or the review by Kull (1991))

$$\lambda = \sqrt{Agk}\,. \tag{4}$$

According to (4), the growth rate increases indefinitely with k, thus favoring the growth of short-wavelength perturbations. Several physical effects can limit the growth at large wavenumbers, including surface tension, viscosity (Chandrasekhar 1961; Menikoff et al. 1977), diffusivity (Duff et al. 1962). Linear stability analysis has been also generalized to include other physical ingredients, including rotation (Chandrasekhar 1961), compressibility (Mitchner & Landshoff 1964), viscoelasticity (Boffetta et al. 2010b), non-uniform acceleration (Kull 1991).

3. Phenomenology of Rayleigh-Taylor turbulence

The linear phase of the instability, discussed in Section 2, breaks down when the amplitude of the perturbation of the interface becomes comparable with the wavelength. At this

Rayleigh-Taylor experiments

Several setups have been proposed for the experimental study of RT turbulence. At variance with, e.g. Rayleigh-Benard convection, for RT turbulence there is not a "standard" setup and several experiments have been proposed to generate the initial state which is, by definition, unstable. Different techniques have been developed to stabilize the initial configuration, starting from the compressed gas experiments by Lewis (1950) in a thin layer. In the Rocket-Rig apparatus of Read (1984) (see also Youngs (1992)) the initial stable configuration (light fluid over heavy fluid) is accelerated downwards by a small rocket motor with an acceleration larger than gravity. The evolution of the instability is limited in time (by the vertical extension of the setup) and this required the use of large Atwood numbers or immiscible fluids (Andrews & Dalziel 2010). A more recent variant of this setup, developed by Dimonte & Schneider (1996) uses a linear electric motor which allows to control the acceleration profile.

The overturning tank developed by Andrews & Spalding (1990) generates the instability by rotating a narrow tank mounted on a horizontal axis. This setup overcomes the problem of small Atwood numbers experiments of the Rocket-Rig apparatus and working fluids are typically fresh water and brine solution with $A \simeq 0.05$. The sliding barrier experiment developed by Linden et al. (1994) uses a removable metal sheet to separate the two layers of fluid at different density (again brine and fresh water). One of the problem with this setup is the generation of viscous boundary layers around the sheet when it is removed. The setup was later improved by Dalziel (1993) who used a nylon fabric wrapped around the metal plate to eliminate the boundary layers. A similar setup, developed by Rivera & Ecke (2006), uses a stretched latex membrane to separate the two layers. When the latex membrane is ruptured with a needle the instability starts. This setup was used for investigating RT mixing at $A \simeq 0.003$ and small aspect ratio (lateral dimensions one fifth the vertical size) and the growth of the mixing layer was found to be slower than t^2.

A different setup, developed by Snider & Andrews (1994), uses a water channel in which two water streams at different densities (temperatures) flow parallel separated by a thin horizontal plate. A the end of the plate the streams enter the test channel where they meet and the RT instability develops. The main advantage of the present setup is that mixing evolves in space and not in time allowing for time averages over a statistically stationary state. The original channel were developed for very small Atwood numbers ($A \sim 10^{-3}$) while a more recent setup developed by Banerjee & Andrews (2006) is capable to reach $A \simeq 1$. Another, and promising technique developed by Huang et al. (2007) makes use of a strong magnetic field gradient to stabilize a paramagnetic (heavy) fluid over a diamagnetic (light) one. In yet another variant, the initial configuration is opposite (and stable) and the magnetic field is used to produce the instability (Baldwin et al. 2015).

point nonlinear effects emerge and the RT flow develops into a different, nonlinear phase. This nonlinear phase is characterized by the formation of ascending and descending plumes which detach from the original region of hot or cold fluid and enter the opposite region, thus enhancing the transport of heat between the two reservoirs. At this point the interface between the two regions is not single valued any more and several modes are activated leading eventually to the turbulent phase.

The phenomenology of the temporal evolution of the turbulent phase can be derived dimensionally starting from the energy equation. Introducing the kinetic energy density

$E = (1/2)\langle|\mathbf{u}|^2\rangle$ (where $\langle ...\rangle$ indicates average over the space), from (2) one obtains

$$\frac{dE}{dt} = \beta g\langle wT\rangle - \varepsilon_\nu = -\frac{dP}{dt} - \varepsilon_\nu \tag{5}$$

where we have introduced the potential energy of the system, $P \equiv -\beta g\langle zT\rangle$ and the viscous energy dissipation rate $\varepsilon_\nu = \nu\langle(\boldsymbol{\nabla u})^2\rangle$. For simplicity, in (5) the (small) contribution of the thermal diffusivity is neglected. By introducing the typical velocity fluctuation U, one has dimensionally from (5)

$$\frac{dU^2}{dt} \simeq \beta g U\theta_0 \tag{6}$$

because the temperature fluctuation at the integral scale is θ_0 and therefore, by integration,

$$U(t) \simeq Agt \tag{7}$$

i.e. the large-scale velocity fluctuation grows linearly in time. Since this is the velocity which moves the plumes within the mixing layer, by integration one obtains the dimensional prediction for the quadratic growth of the layer width $h(t)$

$$h(t) = \alpha Agt^2 \tag{8}$$

where the dimensionless parameter α represents the efficiency of the conversion of potential energy into kinetic energy. The phenomenology of small-scale RT turbulence, which will be discussed in Section 4, assumes that within the mixing layer a turbulent cascade *à la* Kolmogorov develops, with an integral scale h which grows in time according to (8) and an energy flux given dimensionally by $\varepsilon \simeq U^3/h \simeq (Ag)^2 t$.

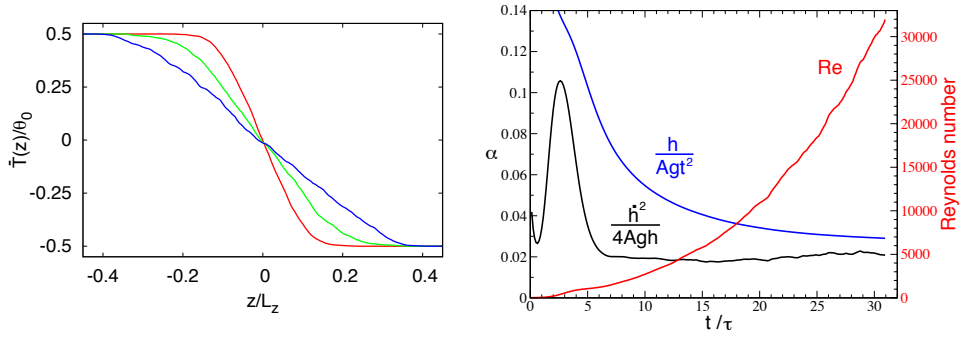

Figure 2

(Left) Mean temperature profile $\overline{T}(z,t)$ at times $t = 1.4\tau$ (red), $t = 2.0\tau$ (green) and $t = 2.6\tau$ (blue) from a numerical simulation of RT turbulence ($\tau = (L_z/Ag)^{1/2}$). (Figure from Boffetta et al. (2009)). (Right) Evolution of the mixing layer thickness $h(t)$ and its growth rate $\dot{h}(t)$ normalized by the Atwood number A, gravity g and time, as a function of time. (Figure from Cabot & Cook (2006)).

Figure 2 shows the mean temperature profile $\overline{T}(z,t)$ as a function of z at different times. The profile is obtained by averaging the temperature field shown in Fig. 1 over the horizontal plane (x,y) and over different realizations of the numerical simulations. It is evident from this plot that the inner region of the mixing layer develops a linear temperature profile $\overline{T}(z,t) \simeq -\gamma(t)z$ with a gradient which dimensionally decreases as $\gamma(t) \simeq \theta_0/h \simeq t^{-2}$

(see Boffetta et al. (2009) for the 3D case and Celani et al. (2006); Biferale et al. (2010); Zhou (2013) in two dimensions). Different definitions of the width of the mixing layer have been proposed, based on either local or global properties of $\overline{T}(z)$. The simplest measure is based on the threshold value h_r at which $\overline{T}(z)$ reaches a fraction r of the maximum value, i.e. $\overline{T}(\pm h_r/2) = \mp r\theta_0/2$ (see, e.g. Dalziel et al. (1999)). Other definitions, proposed by Cabot & Cook (2006) and Vladimirova & Chertkov (2009), are based on integral quantities, i.e. $h_M = \int M(\overline{T})dz$ where M is an appropriate mixing function which has support on the mixing layer only. Linearity of the mean temperature profile implies statistical homogeneity inside the mixing layer, a key ingredient for the development of a phenomenological theory of turbulent fluctuations based on Kolmogorov (1941)(see Section 4). Deviations from this linear profile, with the crossover of $\overline{T}(z)$ to the bulk values $\pm\theta_0/2$ can be indeed understood as a manifestation of non-homogeneity of turbulence at the edge of the mixing layer. These deviations can be captured by a mixing length model with a z-dependent eddy diffusivity as shown by Boffetta et al. (2010a) and Biferale et al. (2011b).

One of the first work which addresses the nonlinear evolution of the interface is due to Fermi & von Neumann (1955). In their unpublished note, they assume a rectangular plume which moves vertically pushed by gravity. In the simplified version of up-down symmetry (Boussinesq approximation) the variation of potential energy given by a couple of plumes (of densities ρ_1 and ρ_2) of square base b^2 and height h moving in the region of different density is

$$\Delta P = (\rho_1 - \rho_2)b^2 g h^2 \tag{9}$$

which is negative as potential energy decreases. If the plumes are moving with constant vertical velocity $\dot{h}$ the change of kinetic energy in the system is

$$\Delta E = \frac{1}{2}(\rho_1 + \rho_2)b^2 h\dot{h}^2 \tag{10}$$

By using the Euler-Lagrange equation $\partial L/\partial h = d/dt(\partial L/\partial \dot{h})$ for the Lagrangian $L = E - 2\alpha P$, one obtains

$$\ddot{h}h + \frac{1}{2}\dot{h}^2 = 4\alpha A g h \tag{11}$$

where α is the same parameter as in (8), here representing (with a factor 2) the fraction of potential energy which is converted into kinetic energy of the plumes (while the fraction $1 - 2\alpha$ is dissipated by viscosity and diffusivity). The solution to (11) for an initial height $h(0) = h_0$ is given by

$$h(t) = h_0 + 2(\alpha A g h_0)^{1/2} t + \alpha A g t^2 \tag{12}$$

When extended from single plume to the whole interface, this solution shows that asymptotically the growth of the mixing layer follows the well-known accelerated law $h(t) = \alpha A g t^2$, but this regime dominates after a transient which lasts up to a time $\propto \left(\frac{h_0}{\alpha A g}\right)^{1/2}$.

Recently, the Fermi & von Neumann (1955) result (11) has been rediscovered by different authors and using different arguments. Ristorcelli & Clark (2004) used a self-similar analysis of the Navier-Stokes equation, while Cook et al. (2004) used a mass flux and energy balance argument. They both obtain the same equation for the growth of the mixing width h

$$\dot{h}^2 = 4\alpha A g h \tag{13}$$

which is a particular case of (11) and admits the same solution (12).

One useful application of this approach is for data analysis in order to measure the dimensionless coefficient α. The determination of α and its possible universality has been indeed object of many studies. The picture which emerges is that the measurement of α from the fit of $h(t)$ with t^2 is sensitive to the transient behavior which depends on the initial perturbation of the interface. It has been found that, in general, experimental measurements give a value of α in the range $0.05-0.07$ (Snider & Andrews 1994; Read 1984; Dimonte & Schneider 1996; Linden et al. 1994; Schneider et al. 1998; Banerjee & Andrews 2006) while numerical simulations report lower values around 0.03 (Cabot & Cook 2006; Vladimirova & Chertkov 2009; Dimonte et al. 2004; Young et al. 2001; Youngs 1991). One possible origin of this difference is due to the presence of long wavelength perturbations in the experiments, while numerical simulations are usually perturbed at small scales. Indeed, when these longwave perturbations are present in the initialization of the simulations, the results are closer to the experiments. The basic idea of this approach is to use directly (13), i.e. to measure α as $\alpha = \dot{h}^2/(4Agh)$ instead of $\alpha = h/(Agt^2)$. The comparison of the two methods is shown in Fig. 2 which shows that the "similarity method" converges to a constant value of α much faster than the standard method. The slow convergence of $h/(Agt^2)$ (due to the presence of the constant and linear terms in (12)) is probably one of the reasons why different simulations, characterized by different Reynolds numbers (i.e. resolutions) give different results for the value of α.

3.1. Global heat transfer scaling

Rayleigh-Taylor turbulence represents an example of turbulent thermal convection in which heat is transferred, thanks to the work done by buoyancy forces, between cold (heavy) and hot (light) portion of fluid. The transfer of heat in RT turbulence is inherently associated to the presence of turbulence, as the turbulent layer, during its growth, penetrates and mixes the two reservoirs of fluids at different temperatures. In this sense, thermal transfer in RT turbulence is very different from the phenomenology observed in Rayleigh-Bénard turbulence, probably the most studied prototype of turbulent convection (see, for example, the reviews by Siggia (1994), Bodenschatz et al. (2000) and Lohse & Xia (2010)). Without entering into details, we recall that the heat transfer in Rayleigh-Bénard convection is dominated by the physics at the boundary layers (both thermal and kinetic) which develop in correspondence of the two plates. Those boundary layers, together with the large-scale convective motion, are responsible of the transfer of heat between the two plates and different regimes have been identified according to the dominant contribution (thermal or kinetic boundary layer or bulk) (Grossmann & Lohse 2000; Ahlers et al. 2009).

In general, the dimensionless measure of the heat transfer efficiency is given by the Nusselt number Nu, defined as the ratio of the global turbulent heat transfer to the molecular one, while turbulence intensity is measured, as usual, by the Reynolds number Re. These two numbers depend on the control parameters which are the Rayleigh number Ra (a dimensionless measure of the temperature difference which forces the system) and the Prandtl number $Pr = \nu/\kappa$. A basic problem in thermal convection is the characterization of the state of the system as a function of the parameters, i.e. the functional relation $Nu(Ra, Pr)$ and $Re(Ra, Pr)$. Many experimental (Niemela et al. 2000; Funfschilling et al. 2009) and numerical (Stevens et al. 2010) studies, supported by theoretical arguments (Siggia 1994; Grossmann & Lohse 2000; Ahlers et al. 2009) show that, for Rayleigh numbers much larger

than the critical for the onset of convection, a scaling regime develops under which

$$Nu \simeq Ra^{\gamma} Pr^{\delta} \quad Re \simeq Ra^{\gamma'} Pr^{\delta'} \tag{14}$$

Several theories have been proposed to predict the values of the scaling exponents in (14) in Rayleigh-Bénard convection (see the review by Siggia (1994) and Ahlers et al. (2009)). Without entering into details, we mention that recent experimental and numerical data, characterized by a wide extension in the parameter space and high precision, show that probably the heat transfer in Rayleigh-Bénard convection cannot be captured by simple scaling laws and this phase diagram in the (Ra, Pr) space is more complex than expected (Grossmann & Lohse 2000; Ahlers et al. 2009).

One "fixed point" in the space of the theories on turbulent convection is that, for large enough Rayleigh number, the effects of boundary layers disappear and a transition to a new regime dominated by bulk contributions occurs. This regime, first predicted by Kraichnan (1962) and later discussed by Spiegel (1971), is known as the *ultimate state* of thermal convection, and is characterized by the simple set of scaling exponents $\gamma = \delta = \gamma' = 1/2$, $\delta' = -1/2$. In spite of the large body of experimental and numerical efforts, the ultimate regime remained elusive in Rayleigh-Bénard convection, even at the largest Ra number achieved. On the contrary, it has been observed both in numerical simulations of convection in the absence of boundaries by Lohse & Toschi (2003) and in laboratory experiments in convective cells with elongated geometries which reduce the effects of upper and lower walls by Gibert et al. (2006) and by Cholemari & Arakeri (2009).

The above discussion suggests that RT turbulence is a good candidate to observe the ultimate regime. No boundary layers are indeed present in the RT system. The ultimate state scaling emerges from the energy balance (5). The appropriate definition of the Rayleigh number is in terms of the mixing layer height h as $Ra \equiv \beta g \theta_0 h^3/(\nu\kappa)$, while the Reynolds and the Nusselt number are respectively $Re \equiv Uh/\nu$ (U is a typical large-scale velocity) and $Nu = \langle wT \rangle h/(\kappa\theta_0)$. We can rewrite (5) as

$$\kappa \frac{\beta g \theta_0}{h} Nu = \frac{d}{dt} \frac{1}{2} \langle u^2 \rangle + \varepsilon_\nu \tag{15}$$

By using the dimensional behavior (7-8) for $h(t)$ and $U(t)$ we obtain the temporal behavior $Nu \simeq (\beta g \theta_0)^2 t^3/\kappa$. From the above definition of the Rayleigh number we have $Ra \simeq (\beta g \theta_0)^4 t^6/(\nu\kappa)$ and therefore

$$Nu \simeq Ra^{1/2} Pr^{1/2} \tag{16}$$

Similarly, from the definition of the Reynolds number we have $Re \simeq (\beta g \theta_0)^2 t^3/\nu$ and thus

$$Re \simeq Ra^{1/2} Pr^{-1/2} \tag{17}$$

We remark that the energy balance leading to (15) is independent of the dimensionality and therefore the ultimate state regime is expected to hold also in 2D RT turbulence despite the fact that in this case the energy flows to large scales (and hence $\varepsilon_\nu = 0$) generating a different spectrum (see Section 4).

The functional dependence $Nu(Ra, Pr)$ and $Re(Ra, Pr)$ obtained from direct numerical simulations of RT turbulence at high resolution are shown in Fig. 3. Several simulations, characterized by different Pr numbers, have been performed starting from the same initial condition. Numerical data for the Nusselt number Nu are compatible with the scaling (16) for $Ra > 10^7$ and for $0.2 \leq Pr \leq 10$. Some statistical fluctuations are observed, in particular

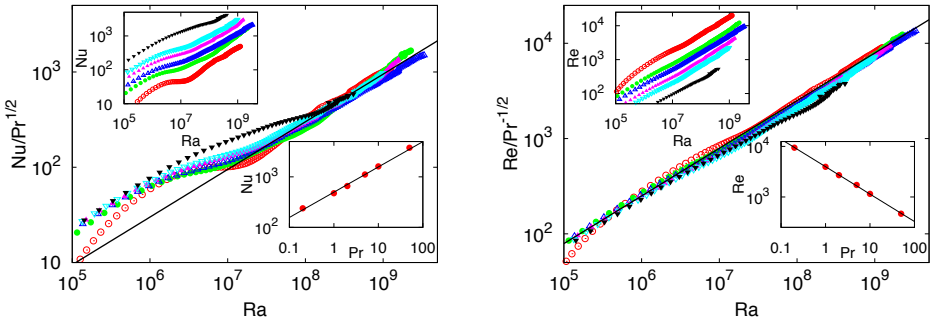

Figure 3

Nusselt (Nu, left) and Reynolds (Re, right) numbers as a function of Rayleigh number Ra from a set of direct numerical simulations of RT turbulence at different Prandtl number: $Pr = 0.2$ (red open circles), $Pr = 1.0$ (green closed circles), $Pr = 2.0$ (blue open upper triangles), $Pr = 5.0$ (pink closed upper triangles), $Pr = 10.0$ (cyan open lower triangles) and $Pr = 50.0$ (black closed lower triangles). The line in the main plot represents $Ra^{1/2}$ scaling. Lower insets: Nu (left) and Re (right) vs Pr at fixed $Ra = 3 \times 10^8$. The lines in the insets represent the best fit exponents 0.51 (left) and -0.54 (right). Figure taken from Boffetta et al. (2012b).

for high Pr. The inset in Fig. 3 shows the dependence on Pr obtained by computing Nu at fixed Ra. The best fit gives a slope 0.51 ± 0.02, compatible with (16). The analysis for the Reynolds number shows a similar result, marginally compatible with (17) for $Ra > 10^6$. At variance with Nu, here the dependence on Pr gives a best fit slope (-0.54 ± 0.01) which deviates from the theoretical prediction. The origin of this small deviation is unknown, but it could originate from finite size effects which affect the definition of integral quantities.

4. Two-point statistical observables

Two-point statistical observables, which involve averaged field differences between couple of points, are key observables in turbulence (see, e.g., Frisch (1995) and Sreenivasan & Antonia (1997)) since they are linked to experimentally measurable scale-dependent quantities as, by way of example, the kinetic energy spectrum or the potential energy spectrum in gravity driven flows. A long-standing challenge in RT turbulence is to determine universal scaling laws for inertial range two-point statistics, as done by Kolmogorov (1941) in ideal hydrodynamics turbulence.

Different theories for turbulent fluctuations have been proposed for RT turbulence over the years. Chertkov (2003) analyzed the advanced mixing regime of the RT turbulence in the small Atwood number Boussinesq approximation. A Kolmogorov–Obukhov (in short, K41) scenario for velocity and temperature spectra is predicted in three dimensions while a Bolgiano–Obukhov (in short, BO59) scenario is shown to arise in two dimensions. Mikaelian (1989) derived the turbulent energy and its spectrum in the Canuto–Goldman model (Canuto & Goldman 1985) when the turbulence is generated by an instability having a power-law growth rate. This model does not predict a Kolmogorov spectrum. For quantitative results in this respect see the paper by Soulard et al. (2015).

Zhou (2001) proposed a modification of the classical Kolmogorov framework by substituting the time-scale for the decay of transfer function correlations, resulting from nonlinear

interactions, with the typical time-scale arising from the linear theory of RT instability, $(kgA)^{-1/2}$. A non Kolmogorov scaling, $k^{-7/4}$, emerges for the energy spectrum. The insertion of a linear time-scale in a fully developed turbulent regime seems however not fully justified. On the basis of symmetries of turbulent dynamics, Abarzhi (2010a) analyzed the influence of momentum transport on the properties of the turbulent RT system. The resulting scaling law is k^{-2} and thus distinct from the Kolmogorov scaling. A similar spectrum was proposed within the "momentum model" by Sreenivasan & Abarzhi (2013). Soulard & Griffond (2012) calculate the anisotropic correction to the isotropic inertial range Kolmogorov scaling in terms of a perturbative approach. This approach is justified on the basis of the numerical evidences found by Boffetta et al. (2009) for 3D RT turbulence showing that, at small scales, the contribution of buoyancy forces to the energy flux becomes much smaller than the contribution of the inertial non-linear forces. Their results do not contradict the theory by Chertkov (2003). Moreover, Soulard (2012) adapted the Monin-Yaglom relation to RT turbulence both in three dimensions, which confirms the Kolmogorov-Obukhov theory, and in two dimensions where it recovers the Bolgiano–Obukhov scenario proposed by Chertkov (2003). Finally, Poujade (2006) proposed a theory, based on a spectral equation, showing that a balance mechanism between buoyancy and spectral energy transfer can settle at low wave numbers in the self-similar regime. The above balance constrained velocity spectrum in a way incompatible with Kolmogorov–Obukhov mechanism. It has however to be pointed out that the theory does not rule out a Kolmogorov-Obukhov scenario at intermediate wave numbers. This proliferation of theoretical models, all reasonable and plausible, are ascribed to the variety of dynamical regimes in RT turbulence mainly due to the non stationarity of the process.

The phenomenological theory by Chertkov (2003) consider a mixing layer in the self-similar regime with an integral scale $h(t)$ and large scale velocity $U(t)$ given by (8) and (7) respectively. Starting from these assumptions, for the 3D case Chertkov (2003) proposed a quasi-stationary, adiabatic, generalization of Kolmogorov–Obukhov picture of steady Navier–Stokes turbulence (Kolmogorov 1941; Obukhov 1941). The first step is to assume the existence of an inertial-range of scales characterized by a scale-independent kinetic energy flux, $\varepsilon(t)$, given by the usual K41 relation:

$$\varepsilon(t) = \frac{U(t)^3}{h(t)} \simeq (\beta g \theta_0)^2 t \tag{18}$$

where we neglect the coefficient $\alpha = O(1)$. Because of the explicit time dependence, the assumption of scale-independence is justified only if the variation of the flux, a large-scale quantity, is slow to allow small-scale fluctuations to adjust adiabatically to the current value of the flux (Chertkov 2003). If ε is scale-independent, following the standard Kolmogorov argument one can write $\varepsilon \simeq \frac{\delta_r u^3}{r}$ where $\delta_r u$ is the velocity fluctuation on a scale r belonging to the inertial range $\eta(t) \ll r \ll h(t)$ and η is the analogous of the Kolmogorov's viscous scale, to be determined in the following. By standard power-counting and exploiting (18) one gets:

$$\delta_r u(t) \simeq (\beta g \theta_0)^{2/3} r^{1/3} t^{1/3} \tag{19}$$

The same adiabatic idea extended to temperature fluctuations, $\delta_r T$, which are supposed, as velocity fluctuations, to cascade toward smaller and smaller scales at a constant rate, leads to the generalization of the Obukhov–Corrsin theory (in short OC51) of passive scalar

advection (Obukhov 1949; Corrsin 1951)

$$\epsilon_T(t) \simeq \frac{\theta_0^2 U}{h} \simeq \frac{\delta_r T^2 \delta_r u}{r} \tag{20}$$

valid in the same range of scales of (19). Exploiting (19), the scaling prediction for $\delta_r T$ follows from (20):

$$\delta_r T(t) \simeq \theta_0 (\beta g \theta_0)^{-1/3} r^{1/3} t^{-2/3} \tag{21}$$

By simple power counting it is easy to show from (19) and (21) that temperature fluctuations are passive within the inertial range of scales, i.e. $\varepsilon(t) \gg \beta g \delta_r T \delta_r u$, in accord with the assumption that buoyancy only acts on scales around the integral scale $h(t)$.

The Kolmogorov (viscous) scale $\eta(t)$ is defined as the scale below which the kinetic energy coming from the inertial range is dissipated by viscosity. It is defined by the balance $\delta_\eta u^3/\eta \simeq \nu \delta_\eta u^2/\eta^2$ from which, extending the validity of (19) down to $r = \eta$, one has:

$$\eta(t) \simeq \nu^{3/4} t^{-1/4} (\beta g \theta_0)^{-1/2} \tag{22}$$

This time behavior has been verified via three-dimensional DNS by Ristorcelli & Clark (2004). From Eq. (22) the viscous Kolmogorov time-scale $\tau_\eta \equiv \eta/\delta_\eta u$ is

$$\tau_\eta \simeq (\beta g \theta_0)^{-1} \nu^{1/2} t^{-1/2} \,. \tag{23}$$

Note that $h(t)/\eta(t)$ increases in time as $t^{9/4}$.

Two-dimensional turbulence is characterized by two inviscid conserved quantities, kinetic energy and enstrophy. On the basis of standard arguments valid in 2D hydrodynamic turbulence (Boffetta & Ecke 2012), a double-cascade scenario sets in with energy flowing toward large scales (with respect to the pumping scale) and enstrophy going to small scale. This scenario in not compatible with the argument developed for 3D as the assumption $\varepsilon(t) \gg \beta g \delta_r T \delta_r u$ is violated at large scales.

Chertkov (2003) proposed a new scenario in which buoyancy and velocity fluctuations balance scale by scale. This is the essence of the Bolgiano–Obukhov scenario introduced in the context of Rayleigh–Bérnard convection (Bolgiano 1959; Obukhov 1959; Siggia 1994; Lohse & Xia 2010). In this case, temperature is active at all scales and the resulting scaling laws emerge by balancing

$$\frac{\delta_r u^2}{r} \simeq \beta g \delta_r T \tag{24}$$

with temperature fluctuations cascading toward small scales at a constant rate according to (20). Combining (20) and (24) one obtains the Bolgiano scaling laws for both velocity and temperature fluctuations:

$$\delta_r u \simeq (\beta g \theta_0)^{2/5} r^{3/5} t^{-1/5} \tag{25}$$

$$\delta_r T \simeq \theta_0 (\beta g \theta_0)^{-1/5} r^{1/5} t^{-2/5} \tag{26}$$

together with the prediction for the viscous scale $\eta(t)$ and its associated time-scale $\tau_\eta \equiv \eta/\delta_\eta u$:

$$\eta(t) \simeq (\beta g \theta_0)^{-1/4} \nu^{5/8} t^{1/8} \qquad \tau_\eta \simeq (\beta g \theta_0)^{-1/2} \nu^{1/4} t^{1/4} \tag{27}$$

valid for $\nu \gg \kappa$. The ratio between the integral scale $h(t)$ and the viscous scale $\eta(t)$ now increases as $t^{15/8}$, slower than in 3D.

4.1. Spatial and temporal scaling laws of structure functions and spectra

The scaling relationships (19) and (21), in 3D, and (25) and (26), in 2D, set the dimensional predictions for both velocity and temperature fluctuations in the spatial and temporal domain. Neglecting possible intermittency fluctuations, these predictions can be used to build (dimensional) scaling laws of structure functions and isotropic spectra. For the 3D case, velocity and temperature structure functions and spectra are

$$S_p(r) = \langle \left[(\mathbf{u}(\mathbf{r},t) - \mathbf{u}(\mathbf{0},t)) \cdot \frac{\mathbf{r}}{r} \right]^p \rangle \simeq (\beta g \theta_0)^{2p/3} t^{p/3} r^{p/3} \tag{28}$$

$$E(k) \simeq (\beta g \theta_0)^{4/3} t^{2/3} k^{-5/3} \tag{29}$$

$$S_p^T(r) = \langle [T(\mathbf{r},t) - T(\mathbf{0},t)]^p \rangle \simeq \theta_0^p (\beta g \theta_0)^{-p/3} t^{-2p/3} r^{p/3} \tag{30}$$

$$E_T(k) \simeq \theta_0^2 (\beta g \theta_0)^{-2/3} t^{-4/3} k^{-5/3} \tag{31}$$

while for the 2D case:

$$S_p(r) = \langle \left[(\mathbf{u}(\mathbf{r},t) - \mathbf{u}(\mathbf{0},t)) \cdot \frac{\mathbf{r}}{r} \right]^p \rangle \simeq (\beta g \theta_0)^{2p/5} t^{-p/5} r^{3p/5} \tag{32}$$

$$E(k) \simeq (\beta g \theta_0)^{4/5} t^{-2/5} k^{-11/5} \tag{33}$$

$$S_p^T(r) = \langle [T(\mathbf{r},t) - T(\mathbf{0},t)]^p \rangle \simeq \theta_0^p (\beta g \theta_0)^{-p/5} t^{-2p/5} r^{p/5} \tag{34}$$

$$E_T(k) \simeq \theta_0^2 (\beta g \theta_0)^{-2/5} t^{-4/5} k^{-7/5} \tag{35}$$

In the above expressions, brackets denote space averages within the mixing layer under the hypothesis of small-scale homogeneity and isotropy. Homogeneity actually follows from the observation that the horizontally ensemble-averaged temperature field, $\overline{T}(z)$, behaves linearly along the gravitational direction (see Section 3) together with the fact that the equation for the horizontally ensemble-averaged velocity reduces to $\partial \overline{p}(z)/\partial z = \beta g \overline{T}(z)$. From these two remarks it immediately follows that temperature fluctuations around $\overline{T}(z)$ are homogeneous and the same is for the velocity: this is indeed forced by temperature fluctuations, the horizontally averaged temperature being balanced by the averaged pressure field as stated above. The above scenario is confirmed by a deep analysis on the distribution of the local dissipation scale carried out in two-dimensions by Qiu et al. (2014). The tendency toward isotropy restoration of small-scale fluctuations has been numerically verified by Biferale et al. (2010) in two dimensions and by Boffetta et al. (2009) and Boffetta et al. (2010d) in three dimensions, and by Ramaprabhu & Andrews (2004) in an experimental investigation.

The validity of the BO59 scenario encoded in the scaling relations (32)–(35) has been first addressed by means of DNS in two dimensions by Celani et al. (2006), exploiting a standard pseudo-spectral method, and successively by Biferale et al. (2010) using a thermal lattice Boltzmann method. In the left panels of Figure 4 we report from Celani et al. (2006) the velocity (left) and temperature (right) structure functions of orders $p = 2$, $p = 4$ and $p = 6$. The curves for $p = 2$ closely agree with the Chertkov (2003) theory both for the spatial and for the temporal scaling. A close look at higher orders reveals the presence of non-negligible deviations with respect to the dimensional predictions. The presence of these intermittency corrections have been also confirmed by Biferale et al. (2010) and Zhou (2013). Intermittency was not observed for the velocity structure functions which exhibit, within

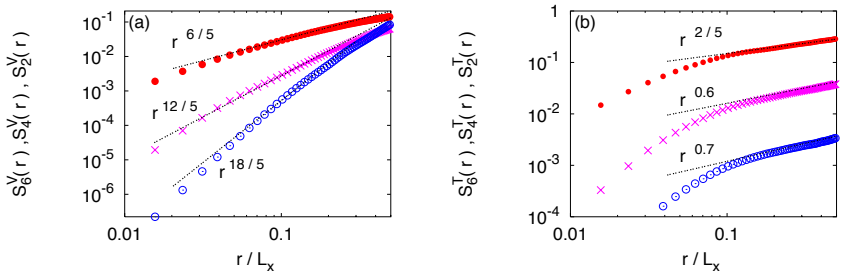

Figure 4

Isotropic moments of the longitudinal velocity differences (a) and temperature differences (b) of order 2 (red full circles), 4 (pink crosses) and 6 (blue empty circles) obtained by averaging over all directions of separation **r**. In plot (a) dashed lines represent the Bolgiano dimensional prediction $S_p(r) \simeq r^{3p/5}$, while in plot (b) scaling exponents for $p = 4$ and $p = 6$ are anomalous. Figure from Celani et al. (2006).

error bars, dimensional scaling, as in the case of the inverse cascade in 2D Navier-Stokes turbulence (Boffetta & Ecke 2012).

It is interesting to note that the set of scaling exponents for velocity and temperature structure functions obtained by Celani et al. (2006) are in remarkable agreement with the scaling exponents found for the 2D turbulent RB system forced by the mean gradient analyzed by Celani et al. (2002). This support the universality of scaling exponents in two systems with different boundary conditions. At the level of spectral observables for both velocity and temperature, the confirmation of the BO59 scaling, both in space and in time, has received a strong support from the numerical simulations by Zhou (2013).

Let us now consider the three-dimensional case. Evidences of energy cascade from large to small length scales with an associated K41 spectrum (for both velocity and density) have been provided by an air-helium gas channel experiment by Banerjee et al. (2010) (see Figure 5). Their observation is consistent with previous measurements in the water channel by Ramaprabhu & Andrews (2004) and Mueschke et al. (2006). However, the mixing layer does not have a sufficient range of scales to make a definitive assessment of the spectral behavior. A detailed analysis based on image processing techniques have been employed by Dalziel et al. (1999) to provide the internal structure and statistics of the concentration field. Concentration power spectra have been analyzed and the Obukhov–Corrsin scenario turned out to be compatible with the experimental observations. A similar conclusion has been drawn by Wilson & Andrews (2002) (Figure 5).

A confirmation of the K41 scenario also arrived from high-resolution numerical simulations. We refer to the numerical simulations by Young et al. (2001), the numerical studies by Dimonte et al. (2004) and Cabot & Cook (2006) and the study by Vladimirova & Chertkov (2009) where it is stated that the range of scales compatible with the Kolmogorov scaling grows with time and that the viscous scale decreases with time in accordance with predictions by Chertkov (2003). A clear $k^{-5/3}$ power law has also been extracted for the vertical velocity spectrum and for the density obtained from accurate LES by Cook et al. (2004).

The advantage of numerical strategies with respect to experiments is that information on the intermittency corrections becomes available. We cite in this respect the works by Matsumoto (2009), Boffetta et al. (2009) and Boffetta et al. (2010d) (see Figure 5). In these

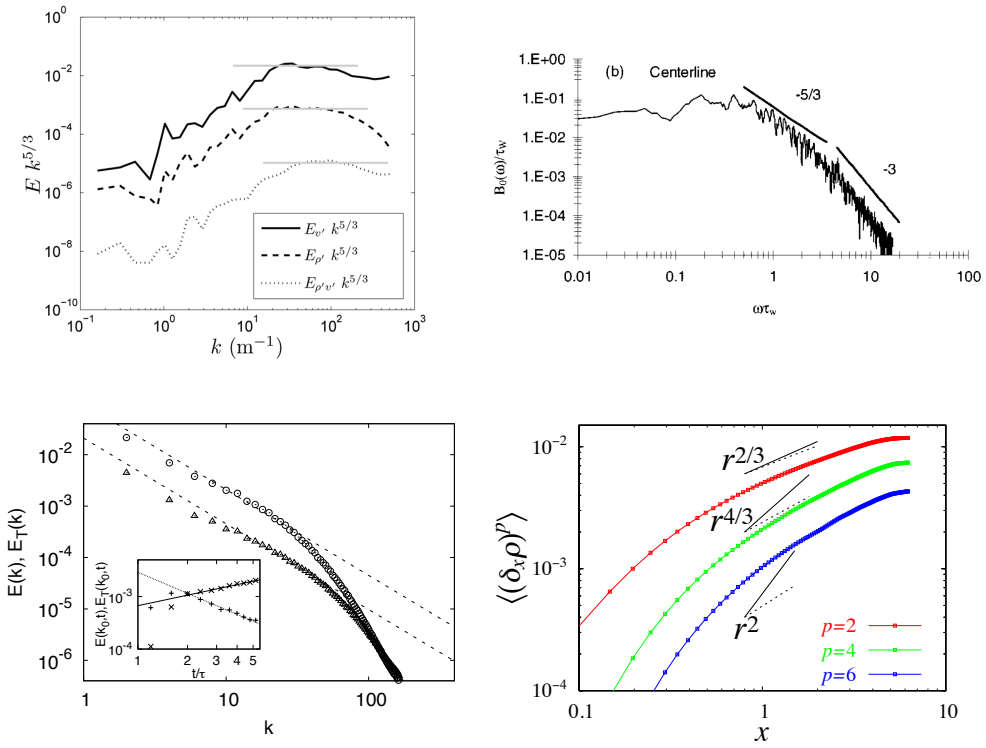

Figure 5

Kinetic energy and density/temperature variance spectra for different Rayleigh-Taylor turbulent flows. Upper left: turbulent kinetic energy spectrum $E_{v'}$, density fluctuations spectrum $E_{\rho'}$ and correlation spectrum $E_{\rho'v'}$ from an air-helium gas experiment at Atwood number $A = 0.03$ (Banerjee et al. 2010). Spectra are compensated with $k^{-5/3}$ to show the range of Kolmogorov scaling. Upper right: density fluctuation spectra from a water experiment at small Atwood number and $Pr = 7$ by Wilson & Andrews (2002). Both the inertial ($-5/3$) and the viscous-convective (-3) regimes are observed. Lower left: Kinetic energy and temperature (density) variance from direct numerical simulations of the Boussinesq equations (Boffetta et al. 2009). The dashed lines represent Kolmogorov scaling. The inset displays the time evolution of the kinetic energy ($\times$) and temperature ($+$) spectra compared with the dimensional predictions $t^{2/3}$ and $t^{-4/3}$ respectively. Lower right: density (temperature) structure functions from direct numerical simulations of the Boussinesq equations (Matsumoto 2009). Solid lines represent the dimensional Kolmogorov predictions $S_p^T(r) \simeq r^{p/3}$, while dashed lines represent the anomalous exponents of a passive scalar with mean scalar gradient (Watanabe & Gotoh 2006). Figures takes from the cited articles.

latter two papers it is shown that scaling exponents of isotropic longitudinal velocity structure functions are indistinguishable from those of Navier-Stokes turbulence at comparable Reynolds number (see, e.g., Warhaft (2000) and Watanabe & Gotoh (2004)), a result in support of the universality of turbulence with respect to the forcing mechanism. A similar conclusion was drawn by Antonelli et al. (2007) for buoyancy-dominated turbulent flows in the atmospheric convective boundary layer.

4.2. Bolgiano scaling and Bolgiano length

We have seen in Section 4 that according to the theory of Chertkov (2003), the Bolgiano scale $L_B = \varepsilon^{5/4}\varepsilon_T^{-3/4}(\beta g)^{-3/2}$ (above which the buoyancy forces overcomes the inertial forces) coincides with the integral scales, $L_B \simeq h$ in three dimensions, while it is the smallest active scale $L_B \simeq \eta$ in two dimensions. Therefore the inertial range of scales $\eta \ll r \ll h$ display K41 scaling in 3D and BO59 scaling in 2D and the Bolgiano scale does not appear explicitly in the range of active scales. The identification of the Bolgiano scale, and of the associated BO59 scaling, is one of the open problems in the study of turbulent convection, in particular for Rayleigh-Benard convection (Lohse & Xia 2010).

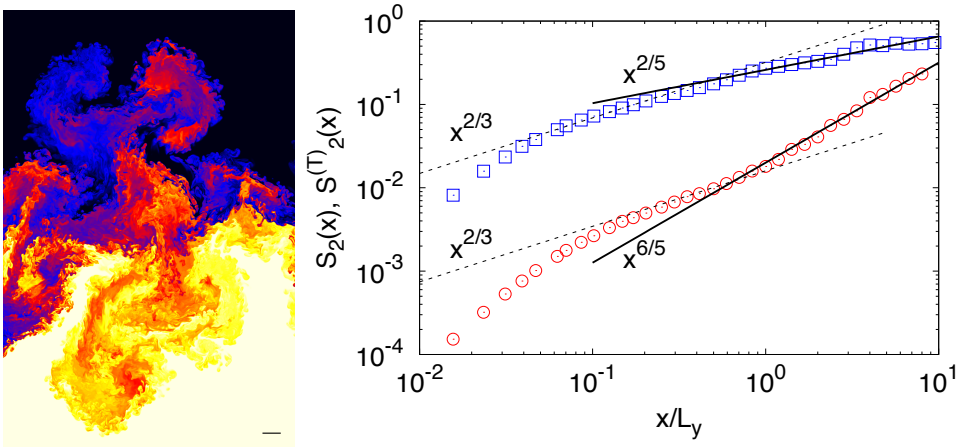

Figure 6

(Left) Vertical section of the temperature field for a simulation of confined RT turbulence at resolution $4096 \times 128 \times 8192$ with aspect ratio $L_y/L_x = 1/32$, $L_z/L_x = 2$. Quasi-two-dimensional plumes are evident at large scales, together with small scale three-dimensional fluctuations. The small black bar represents the dimension L_y of the confining transverse direction. (Right) Second order velocity (red circles) and temperature (blue squares) structure functions computed in the central part of the mixing layer shown on the left. Dotted lines represent Kolmogorov scaling $x^{2/3}$ expected for small scale (below L_y) fluctuations. Solid lines show Bolgiano scaling $x^{6/5}$ and $x^{2/5}$ (for velocity and temperature SF respectively) predicted for scales $x > L_y$.

The idea of Boffetta et al. (2012a) is that the Bolgiano scale could emerge in the inertial range by considering a configuration intermediate between 2D and 3D. This simple idea has been verified by Boffetta et al. (2012a) by means of high-resolution direct numerical simulations of a geometrically confined turbulent RT system with one side, L_y, much smaller than the other two, L_x and L_z. At small times, when $h(t) \ll L_y$, the dynamics is purely three-dimensional. When the mixing layer length becomes larger than L_y, the system is effectively two-dimensional at large scale. The scale L_y is thus expected to be the Bolgiano length of the system, at which a transition from K41 to BO59 occurs. This is shown in Figure 6. In the left panel we report a vertical section $(x - z)$ of the temperature field where large-scale 2D structures coexist with small-scale 3D turbulence. The presence of two different scaling regimes is displayed in the right panel where structure functions for both velocity and temperature fluctuations are shown. Note that the crossover between the two scalings appears at L_y which is therefore identified as the Bolgiano scale of the system.

We conclude this section by recalling that the effects of geometrical confinement in RT turbulence can be even more dramatic when two dimensions are confined (in a quasi-one-dimensional geometry). In this case also large scale quantities are affected by the confinement: for example the width of the mixing layer $h(t)$ displays an anomalous, sub-diffusive growth as observed experimentally by Dalziel et al. (2008) and numerically by Lawrie & Dalziel (2011) and by Boffetta et al. (2012c).

5. Viscoelastic Rayleigh-Taylor turbulence

Polymer additives produce dramatic effects on turbulent flows, the most important being the reduction of turbulent drag up to 80 % when few parts per million of long-chain polymers are added to water (Virk 1975). The natural framework of drag-reduction studies is the case of pipe flow or channel flow: within this context, the reduction of the frictional drag manifests as an increase of the mean flow across the pipe or channel at given pressure drop. In turbulent convection, together with mass, also heat is transported by the flow, therefore an intriguing question is whether also turbulent heat transport is affected, and in particular if it can be enhanced by the presence of polymers. This issue has been addressed only in recent years within the framework of Rayleigh-Benard turbulent convection. These recent studies have shown that, in the range of Ra numbers investigated where the contribution to the dissipation rates from the boundary layers are significant, polymers reduce the global heat transport by a small amount as found in the experiments by Ahlers & Nikolaenko (2010). An enhancement of the heat transport has been observed locally by Xie et al. (2015) within the bulk region of turbulent thermal convection, where the effects of boundary layers is negligible and also in numerical simulations by Benzi et al. (2010) of homogeneous convection, in which boundaries have been removed. It is therefore natural to investigate if and how polymer additives affect the dynamics of RT turbulence. Indeed, the development of the mixing layer implies a vertical transport of mass under the effect of gravity which has analogies with the transport in the channel under pressure forces. Moreover, the absence of boundary layers in the development of RT turbulence suggests that the effects of polymer additives can be very different with respect to the case of RB convection.

Theoretical studies of polymer additives in turbulence are usually based on viscoelastic models in which polymer effects are embodied in a positive symmetric conformation tensor $\sigma(\mathbf{x},t) = \langle \mathbf{RR} \rangle / R_0^2$ representing the local polymer elongation averaged over the thermal noise (and normalized to the equilibrium length R_0) (Bird et al. 1977). One of the simplest viscoelastic models is the linear Oldroyd-B model which, for the OB framework, reads

$$\begin{aligned} \partial_t \mathbf{u} + \mathbf{u}\cdot\nabla\mathbf{u} &= -\nabla p + \nu\nabla^2\mathbf{u} - \beta\mathbf{g}T + \frac{2\nu\gamma}{\tau_p}\nabla\cdot\sigma \\ \partial_t T + \mathbf{u}\cdot\nabla T &= \kappa\nabla^2 T \\ \partial_t \sigma + \mathbf{u}\cdot\nabla\sigma &= (\nabla\mathbf{u})^T\cdot\sigma + \sigma\cdot(\nabla\mathbf{u}) - \frac{2}{\tau_p}(\sigma - \mathbb{I}) + \kappa_p\nabla^2\sigma \end{aligned} \tag{36}$$

In (36) γ is the zero-shear polymer contribution to the total viscosity $\nu_T = \nu(1+\gamma)$ (which is proportional to the polymer concentration), τ_p is the (longest) polymer relaxation time (i.e. the Zimm relaxation time for a linear chain (Bird et al. 1977)) and κ_p represents a polymer diffusivity needed to prevent numerical instabilities (Sureshkumar & Beris 1995). When the fluid is at rest, polymer conformation tensor relaxes to the equilibrium configuration $\sigma = \mathbb{I}$ which is therefore the initial condition at $t = 0$. As turbulence develops in the mixing layer,

polymers are stretched and produce an elastic stress on the flow proportional to $\nabla \cdot \sigma$.

The presence of polymers changes the energy balance with respect to the Newtonian fluid. The total energy has an additional elastic contribution $\Sigma = \frac{\nu\gamma}{\tau_p}[\langle tr\sigma \rangle - 3]$ and this changes (15) to

$$\kappa \frac{\beta g \theta_0}{h} Nu = \frac{dE}{dt} + \frac{d\Sigma}{dt} + \varepsilon_\nu + \varepsilon_\Sigma \tag{37}$$

where $\varepsilon_\Sigma = 2\Sigma/\tau_p$ is the elastic dissipation.

A first indication on the effects of polymer solution in the development of Rayleigh-Taylor turbulence is provided by the linear stability analysis of viscoelastic RT model (36). It has been shown by Boffetta et al. (2010c) that polymer solution speeds up the linear phase of the RT instability by a factor which increases with the elasticity of the solution (proportional to τ_p). This phenomenon is reminiscent of the polymer drag reduction in pipe flow.

For the nonlinear phase, we assume that initially turbulence follows the three-dimensional K41 scenario described in Section 4.1. The viscous time-scale (23) decreases as $\tau_\eta \simeq (\beta g \theta_0)^{-1} \nu^{1/2} t^{-1/2}$, and therefore the Weisenberg number $Wi \equiv \tau_p/\tau_\eta$, a measure of the relative strength of stretching due to velocity gradients and polymer relaxation, thus grows as $Wi \simeq t^{1/2}$. Therefore, even in the presence of a very small polymer relaxation time τ_p, a *coil-stretch transition* by which polymers become active is thus expected for sufficiently long evolution times.

Let us now consider the two-dimensional case. In this case, the initial dynamics is ruled by the BO scaling according to which the viscous time-scale is now given by (27): $\tau_\eta \simeq (\beta g \theta_0)^{-1/2} \nu^{1/4} t^{1/4}$. Therefore in this case the Weisenberg number decreases in time as $Wi \simeq t^{-1/4}$ and polymers will eventually recover (or remain in) the coiled state.

On the basis of the above dimensional arguments, one may conjecture that viscoelastic effects in three dimensions become more and more relevant as the system evolves. The opposite conclusion can be drawn in two dimensions where the role played by polymers is expected to be transient and to disappear in the late stage of the evolution.

The effect of polymers in RT turbulence has been studied by Boffetta et al. (2010b) and Boffetta et al. (2011) on the basis of direct numerical simulations of the viscoelastic model (36). As a result of these papers, it has been shown that in the viscoelastic case the mixing layer growth is faster than in the Newtonian case. Polymers thus make the transfer of mass more efficient, a fact that amounts to saying that the large-scale mixing is enhanced. The opposite happens for the small-scale mixing: temperature variance has been found to be larger in the viscoelastic case than in the Newtonian case. Thermal plumes are thus more coherent in the viscoelastic case, a fact that is expected to contribute to enhance the heat transfer with respect to the Newtonian case. The temperature variance indeed enters in the definition of Nusselt number (see Section 3.1). It turns out that the effect of polymers is to increase the values attained by Nu and Ra at late time. Both in the Newtonian case and in the viscoelastic one, the ultimate-state scaling $Nu \simeq Ra^{1/2}$ has been observed.

The polymer heat transfer enhancement in RT turbulence can be interpreted in terms of polymer drag reduction between rising and sinking plumes. For the RT turbulent system, a quantitative definition of drag in terms of the dimensionless coefficient α (see Section 3) has been proposed by Boffetta et al. (2011). The increase of α induced by polymers observed by Boffetta et al. (2010b) and Boffetta et al. (2011) has been interpreted as a reduction of the turbulent drag, as the RT viscoelastic system is able to convert more efficiently potential energy into kinetic energy contained in large plumes. Conversely, it turns out

that the turbulent transfer of kinetic energy toward small scales is reduced, thus reducing the viscous dissipation. With respect to Newtonian turbulence, a suppression of small-scale velocity fluctuations is observed and it is accompanied by an increase of kinetic energy of the large-scale velocity components. This is the phenomenology of polymer drag reduction observed in homogeneous, isotropic turbulence (see, e.g. De Angelis et al. (2005)).

6. Rayleigh-Taylor turbulence in the presence of rotation

It is well-established that the Coriolis force in rotating fluids can reduce the instability of a flow. The effect of rotation on Rayleigh-Taylor instability was first considered by Chandrasekhar (1961), who concluded that it slows down the instability, and later extended by Tao et al. (2013) to the nonlinear stage. These predictions have been confirmed by numerical simulations by Carnevale et al. (2002) and more recently by the experiments by Baldwin et al. (2015). The effect of rotation on the turbulent phase is less clear. In the case

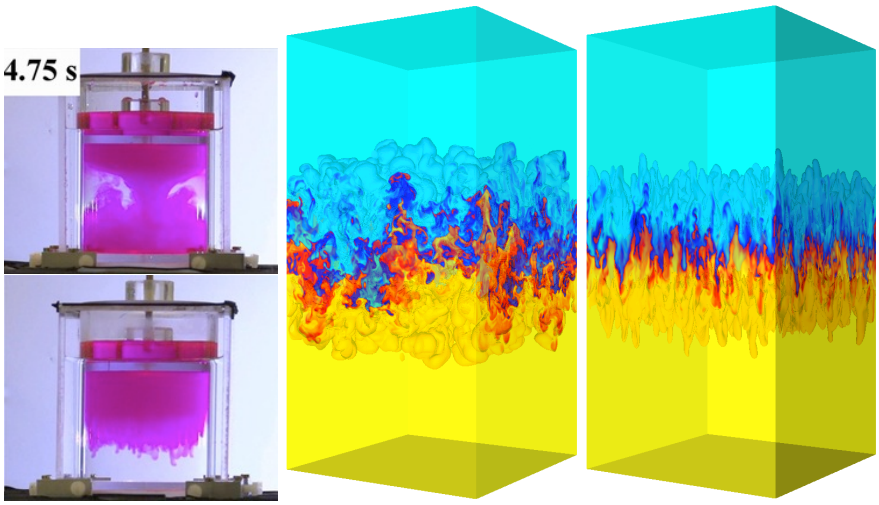

Figure 7

Rotating RT turbulence. The two images on the left show the evolution of the RT instability of a paramagnetic liquid (pink) above a diamagnetic liquid (clear) without rotation (upper) and with $\Omega = 4.6\, rad\, s^{-1}$ (lower) (Figure taken from Baldwin et al. (2015)). The two images on the right represent the temperature field, at the same time $t = 20\tau$, for two simulations of the OB equations with the Coriolis force starting from the same initial condition, with $\Omega = 0$ (left) and with $\Omega\tau = 20$ (right) ($\tau = (L_z/Ag)^{1/2}$).

of Rayleigh-Benard convection it has been shown that turbulence can increase the vertical heat transfer at moderate rotation (and Rayleigh number) by enhancing the Ekman pumping of temperature from the boundaries. For stronger rotation, the bidimensionalization of the flow by the Taylor-Proudmann effect (Tritton 1988) reduces the vertical flow and the heat transfer. As Rayleigh-Taylor has no boundary layers, we expect that here rotation suppresses monotonically the vertical transfer of heat.

The effect of rotation on RT turbulence can be studied, in the OB framework, by adding the Coriolis force $2\boldsymbol{\Omega} \times \mathbf{u}$ (with $\boldsymbol{\Omega} = (0, 0, \Omega)$) to (2). The dimensionless Rossby number $Ro = U/(2\Omega h)$, which measures the relative strength of the inertial forces to the

Coriolis force, here is found to decrease, using (7-8), as $Ro \simeq 1/(\Omega t)$. Therefore the effect of rotation, even if negligible at the initial time, becomes more important and competes with the inertial, and buoyancy, forces for $t \gtrsim 1/\Omega$. Figure 7 shows that the effect of rotation is evident already at a qualitative level with the deformation of the thermal plumes which become elongated as a manifestation of the Taylor-Proudman theorem. The suppression of vertical fluctuations causes a reduction in the growth of the mixing layer which is found to be monotonic in Ω. Therefore, from the discussion in Section 3.1 the evolution of both Ra and Nu (proportional to h^3 and h respectively) is slowed down by rotation. Moreover the turbulent heat transfer is reduced by rotation also at a given Ra: as a consequence of the suppression of the vertical fluctuations, the correlation $\langle wT \rangle$ is reduced with respect to the non-rotating case.

7. Reactive Rayleigh-Taylor turbulence

Recently there has been an increasing interest in reactive RT turbulence which finds applications in several natural phenomena and technological applications, as discussed in the Introduction. Without entering into details, we address here only the general question of how reaction affects the phenomenology of RT turbulence. In particular, the competition between gravitational forces, which mixes the two fluids and produces a mixing layer with uniform temperature, and combustion which produces a propagating front which works against mixing. Vladimirova & Rosner (2003) study the effect of turbulence on the speed

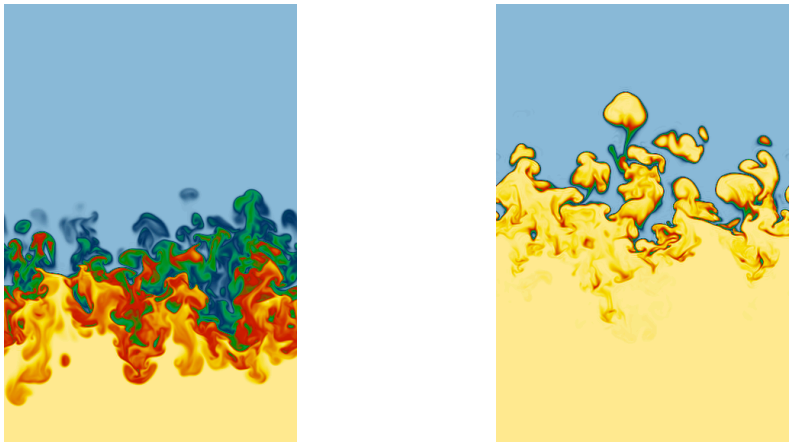

Figure 8

Reactive RT turbulence. Vertical sections of the temperature field at time $t = 128$ for two 3D simulations of RT turbulence with different reaction times: $\tau_r = 1600 \gg t$ (left) and $\tau_r = 16 \ll t$ (right). Observe vertical shift of the mixing layer due to the propagation of the reaction. Image: courtesy of N. Vladimirova.

of a front propagating vertically against gravity by two-dimensional simulations in an elongated domain. Chertkov et al. (2009) extended these simulations to an unconfined domain (with periodic boundary conditions) with a FKPP reaction model (Fisher 1937) characterized by a reaction time τ_r, while Hicks (2015) used a different reaction linearly stable at the ignition temperature. The peculiarity of RT turbulence, with respect to other ex-

amples of turbulent combustion, is that here the ratio of the turbulent mixing time T to the reaction time (the so-called Damköler number $Da = T/\tau_r$) grows linearly in time as $T \simeq h(t)/U(t) \simeq t$. Therefore, even in the case of *slow reaction*, the system will undergo a transition to the *fast reaction* regime $Da > 1$ in which a new *segregated stage* appears. In this new regime, the mixing layer is characterized by the presence of pure phase, shown in Fig. 8, as the turbulent temperature fluctuations have been eliminated by combustion and separated by a thin active interface. Similar results have been obtained by Biferale et al. (2011a) and by Hicks & Rosner (2010) for the two-dimensional case. One interesting result of these investigations is that, in spite of the strong effects on the distribution of the temperature field (which is already evident from Fig. 8), the amplitude and the speed of the mixing layer is weakly affected by the reaction. The main effect in the fast reaction regime is a vertical drift of the mixing layer due to the propagation of the front.

SUMMARY POINTS

1. The development of a direct cascade of energy in the mixing layer with Kolmogorov-Obukhov spectrum is well established by experiments and numerical simulations.
2. In two dimensions, numerical simulations and theoretical arguments support the presence of an inverse cascade of energy with Bolgiano-Obukhov scaling, with temperature fluctuations injecting energy at all scales.
3. RT turbulence undergoes a transition from a three- to two-dimensional phenomenology when the width of the mixing layer becomes larger than the scale of confinement. This latter is identified with the Bolgiano scale.
4. RT system provides a natural realization of the ultimate state of thermal convection thus highlighting the relationship between the absence of boundary layers and the emergence of the ultimate state scaling, both in two and three dimensions.
5. Heat transfer in the RT convection can be enhanced via polymer additives. This phenomenon is accompanied by a speed-up of the mixing layer growth.

FUTURE ISSUES

1. A challenge for future experiments is to measure small-scale velocity and temperature fluctuations, both in two- and in three-dimensional configurations and to identify the Bolgiano scale in confined experiments.
2. Experiments in viscoelastic RT mixing should confirm the enhancement of heat transfer observed in simulations and clarify the differences between RT and RB in this respect.
3. A better understanding of the effect of rotation on RT turbulence is important for astrophysical applications.
4. A better understanding of the role of surface tension for immiscible RT turbulence with the verification of the theoretical predictions.
5. Theoretical, numerical and experimental studies of RT turbulence and mixing of complex particles.

DISCLOSURE STATEMENT

The authors are not aware of any affiliations, memberships, funding, or financial holdings that might be perceived as affecting the objectivity of this review.

ACKNOWLEDGMENTS

We would like to thank Luca Biferale, Alessandro Bottaro, Antonio Celani, Filippo De Lillo, Stefano Musacchio, and Lara Vozella for fruitful collaborations and extensive discussions about Rayleigh-Taylor turbulence. The authors also thank Arindam Banerjee, Andrew Cook, Takeshi Matsumoto and Natalia Vladimirova for help in providing their figures. A. Mazzino thanks the financial support from PRIN 2012 (project n. D38C1300061000 funded by the Italian Ministry of Education) and the Italian flagship project RITMARE.

LITERATURE CITED

Abarzhi S. 2010a. On fundamentals of Rayleigh-Taylor turbulent mixing. *Europhys. Lett.* 91:35001

Abarzhi S. 2010b. Review of theoretical modelling approaches of Rayleigh–Taylor instabilities and turbulent mixing. *Phil. Trans. R. Soc. Lond. A* 368:1809–1828

Agee E. 1975. Some inferences of eddy viscosity associated with instabilities in the atmosphere. *J. Atmos. Sci.* 32:642–646

Ahlers G, Grossmann S, Lohse D. 2009. Heat transfer and large scale dynamics in turbulent Rayleigh–Bénard convection. *Rev. Mod. Phys.* 81:503

Ahlers G, Nikolaenko A. 2010. Effect of a Polymer Additive on Heat Transport in Turbulent Rayleigh-Bńard Convection . *Phys. Rev. Lett.* 104:034503

Andrews M, Dalziel S. 2010. Small Atwood number Rayleigh–Taylor experiments. *Phil. Trans. R. Soc. A* 368:1663–1679

Andrews M, Spalding D. 1990. A simple experiment to investigate two-dimensional mixing by Rayleigh-Taylor instability. *Phys. Fluids A* 2:922–927

Antonelli M, Lanotte A, Mazzino A. 2007. Anisotropies and universality of buoyancy-dominated turbulent fluctuations: a large-eddy simulation study. *J. Atmos. Sci.* 64:2642–2656

Baldwin K, Scase M, Hill R. 2015. The Inhibition of the Rayleigh–Taylor Instability by Rotation. *Sci. Rep.* 5:11706

Banerjee A, Andrews M. 2006. Statistically steady measurements of Rayleigh-Taylor mixing in a gas channel. *Phys. Fluids* 18:035107

Banerjee A, Kraft W, Andrews M. 2010. Detailed measurements of a statistically steady Rayleigh–Taylor mixing layer from small to high Atwood numbers. *J. Fluid Mech.* 659:127–190

Bell J, Day M, Rendleman C, Woosley S, Zingale M. 2004. Direct Numerical Simulations of Type Ia Supernovae Flames. II. The Rayleigh–Taylor Instability. *Astrophys. J.* 608:883

Bellman R, Pennington R. 1954. Effects of surface tension and viscosity on Taylor instability. *Phys. Rev. Lett.* 12:151–162

Benzi R, Ching E, De Angelis E. 2010. Effect of Polymer Additives on Heat Transport in Turbulent Thermal Convection. *Phys. Rev. Lett.* 104:024502

Biferale L, Mantovani F, Sbragaglia M, Scagliarini A, Toschi F, Tripiccione R. 2010. High resolution numerical study of Rayleigh–Taylor turbulence using a thermal lattice Boltzmann scheme. *Phys. Fluids* 22:115112

Biferale L, Mantovani F, Sbragaglia M, Scagliarini A, Toschi F, Tripiccione R. 2011a. Reactive Rayleigh-Taylor systems: Front propagation and non-stationarity. *Europhys. Lett.* 94:54004

Biferale L, Mantovani F, Sbragaglia M, Scagliarini A, Toschi F, Tripiccione R. 2011b. Second-order closure in stratified turbulence: Simulations and modeling of bulk and entrainment regions. *Phys. Rev. E* 84:016305

Bird R, Armstrong R, Hassager O, Curtiss C. 1977. Dynamics of polymeric liquids, vol. 1. Wiley New York

Bodenschatz E, Pesch W, Ahlers G. 2000. Recent developments in Rayleigh-Bénard convection. *Annu. Rev. Fluid Mech.* 32:709–778

Boffetta G, De Lillo F, Mazzino A, Musacchio S. 2012a. Bolgiano scale in confined Rayleigh–Taylor turbulence. *J. Fluid Mech.* 690:426–440

Boffetta G, De Lillo F, Mazzino A, Vozella L. 2012b. The ultimate state of thermal convection in RayleighTaylor turbulence. *Physica* 241D:137–140

Boffetta G, De Lillo F, Musacchio S. 2010a. Nonlinear diffusion model for Rayleigh-Taylor mixing. *Phys. Rev. Lett.* 104:034505

Boffetta G, De Lillo F, Musacchio S. 2012c. Anomalous diffusion in confined turbulent convection. *Phys. Rev. E* 85:066322

Boffetta G, Ecke R. 2012. Two-Dimensional Turbulence. *Ann. Rev. Fluid Mech.* 44:427–451

Boffetta G, Mazzino A, Musacchio S. 2011. Effects of polymer additives on Rayleigh-Taylor turbulence. *Phys. Rev. E* 83:056318

Boffetta G, Mazzino A, Musacchio S, Vozella L. 2009. Kolmogorov scaling and intermittency in Rayleigh–Taylor turbulence. *Phys. Rev. E* 79:065301

Boffetta G, Mazzino A, Musacchio S, Vozella L. 2010b. Polymer heat transport enhancement in thermal convection: The case of Rayleigh-Taylor turbulence. *Phys. Rev. Lett.* 104:184501

Boffetta G, Mazzino A, Musacchio S, Vozella L. 2010c. Rayleigh–Taylor instability in a viscoelastic binary fluid. *J. Fluid Mech.* 643:127–136

Boffetta G, Mazzino A, Musacchio S, Vozella L. 2010d. Statistics of mixing in three-dimensional Rayleigh–Taylor turbulence at low Atwood number and Prandtl number one. *Phys. Fluids* 22:035109

Bolgiano R. 1959. Turbulent spectra in a stably stratified atmosphere. *J. Geophys. Res.* 64:2226–2229

Cabot W, Cook A. 2006. Reynolds number effects on Rayleigh–Taylor instability with possible implications for type Ia supernovae. *Nat. Phys.* :562

Canuto V, Goldman I. 1985. Analytical Model for Large-Scale Turbulence. *Phys. Rev. Lett.* 54:430–433

Carnevale G, Orlandi P, Zhou Y, Kloosterziel R. 2002. Rotational suppression of Rayleigh–Taylor instability. *J. Fluid Mech.* 457:181–190

Celani A, Matsumoto T, Mazzino A, Vergassola M. 2002. Scaling and Universality in Turbulent Convection. *Phys. Rev. Lett.* 88:054503

Celani A, Mazzino A, Muratore-Ginanneschi P, Vozella L. 2009. Phase-field model for the Rayleigh–Taylor instability of immiscible fluids. *J. Fluid Mech.* 622:115–134

Celani A, Mazzino A, Vozella L. 2006. Rayleigh–Taylor Turbulence in Two Dimensions. *Phys. Rev. Lett.* 96:134504

Chandrasekhar S. 1961. Hydrodynamics and Hydromagnetic Stability. Oxford university press

Chang C. 1959. Dynamic instability of accelerated fluids. *Phys. Fluids* 2:656–663

Chertkov M. 2003. Phenomenology of Rayleigh-Taylor Turbulence. *Phys. Rev. Lett.* 91:115001

Chertkov M, Kolokolov I, Lebedev V. 2005. Effects of surface tension on immiscible Rayleigh-Taylor turbulence. *Phys. Rev. E* 71:055301

Chertkov M, Lebedev V, Vladimirova N. 2009. Reactive Rayleigh–Taylor turbulence. *J. Fluid Mech.* 633:1–16

Cholemari M, Arakeri J. 2009. Axially homogeneous, zero mean flow buoyancy-driven turbulence in a vertical pipe. *J. Fluid Mech.* 621:69–102

Cook A, Cabot W, Miller P. 2004. The mixing transition in RayleighTaylor instability. *J. Fluid Mech.* 511:333–362

Corrsin S. 1951. On the spectrum of isotropic temperature fluctuations in an isotropic turbulence. *J. Applied Phys.* 22:469–473

Dalziel S. 1993. Rayleigh-Taylor instability: experiments with image analysis. *Dyn. Atmos. Oceans* 20:127–153

Dalziel S, Linden P, Youngs D. 1999. Self-similarity and internal structure of turbulence induced by Rayleigh–Taylor instability. *J. Fluid Mech.* 399:1–48

Dalziel S, Patterson M, Caulfield C, Coomaraswamy I. 2008. Mixing efficiency in high-aspect-ratio Rayleigh–Taylor experiments. *Phys. Fluids* 20:065106

De Angelis E, Casciola C, Benzi R, Piva R. 2005. Homogeneous isotropic turbulence in dilute polymers. *J. Fluid Mech.* 531:1–10

Dimonte G, Schneider M. 1996. Turbulent Rayleigh-Taylor instability experiments with variable acceleration. *Phys. Rev. E* 54:3740

Dimonte G, Youngs D, Dimits A, Weber S, Marinak M, et al. 2004. A comparative study of the turbulent Rayleigh–Taylor instability using high-resolution three-dimensional numerical simulations: the Alpha-Group collaboration. *Phys. Fluids* 16:1668–1693

Drazin P, Reid W. 1981. Hydrodynamic Stability. Cambridge university press

Duff R, Harlow F, Hirt C. 1962. Effects of diffusion on interface instability between gases. *Phys. Fluids* 5:417–425

Fermi E, von Neumann J. 1955. Taylor instability of incompressible liquids. *Los Alamos Sci. Lab. Rep.* AECU2979

Fisher R. 1937. The wave of advance of advantageous genes. *Ann. Eugenics* 7:355–369

Frisch U. 1995. Turbulence: the legacy of AN Kolmogorov. Cambridge university press

Funfschilling D, Bodenschatz E, Ahlers G. 2009. Search for the ultimate state in turbulent Rayleigh-Bénard convection. *Phys. Rev. Lett.* 103:014503

Garabedian P. 1957. On Steady-State Bubbles Generated by Taylor Instability. *Proc. R. Soc. Lond. A* 241:423–431

Gibert M, Pabiou H, Chilla F, Castaing B. 2006. High-Rayleigh-number convection in a vertical channel. *Phys. Rev. Lett.* 96:084501

Goncharov V. 2002. Analytical Model of Nonlinear, Single-Mode, Classical Rayleigh-Taylor Instability at Arbitrary Atwood Numbers. *Phys. Rev. Lett.* 88:134502

Grossmann S, Lohse D. 2000. Scaling in thermal convection: a unifying theory. *J. Fluid Mech.* 407:27–56

Hecht J, Alon U, Shvarts D. 1994. Potential flow models of Rayleigh-Taylor and Richtmyer-Meshkov bubble fronts. *Phys. Fluids* 6:4019–4030

Hicks E. 2015. Rayleigh-Taylor unstable flames–fast or faster? *Astrophys. J.* 803:72

Hicks E, Rosner R. 2010. Effects of burning on the development of 2D turbulence. *Phys. Scr.* T142:014046

Hillebrandt W, Niemeyer J. 2000. Type Ia Supernova Explosion Models. *Annu. Rev. Astronomy Astrophys.* 38:191–230

Huang Z, De Luca A, Atherton T, Bird M, Rosenblatt C, Carlès P. 2007. Rayleigh-Taylor instability experiments with precise and arbitrary control of the initial interface shape. *Phys. Rev. Lett.* 99:204502

Kilkenny J, Glendinning S, Haan S, Hammel B, Lindl J, et al. 1994. A review of the ablative stabilization of the Rayleigh-Taylor instability in regimes relevant to inertial confinement fusion. *Phys. Plasmas* 1:1379–1389

Kolmogorov A. 1941. The local structure of turbulence in incompressible viscous fluid forvery large Reynolds numbers. *C.R. Acad. Sci. URSS* 30:301–305

Kraichnan R. 1962. Turbulent thermal convection at arbitrary Prandtl number. *Phys. Fluids* 5:1374

Kruskal M, Schwarzschild M. 1954. Some Instabilities of a Completely Ionized Plasma. *Proc. R. Soc. Lond. A* 223:348–360

Kull H. 1991. Theory of the Rayleigh-Taylor instability. *Phys. Rep.* 206:197–325

Lamb H. 1932. Hydrodynamics. Cambridge University Press

Lawrie A, Dalziel S. 2011. Turbulent diffusion in tall tubes. I. Models for Rayleigh-Taylor instability.

Phys. Fluids 23:085109
Lewis D. 1950. The instability of liquid surfaces when accelerated in a direction perpendicular to their planes. II. *Proc. R. Soc. Lond. A* 202:81–96
Linden P, Redondo J, Youngs D. 1994. Molecular mixing in Rayleigh–Taylor instability. *J. Fluid Mech.* 265:97–124
Lohse D, Toschi F. 2003. Ultimate State of Thermal Convection. *Phys. Rev. Lett.* 90:034502
Lohse D, Xia K. 2010. Small-scale properties of turbulent Rayleigh-Bénard convection. *Annu. Rev. Fluid Mech.* 42:335–364
Matsumoto T. 2009. Anomalous scaling of three-dimensional Rayleigh-Taylor turbulence. *Phys. Rev. E* 79:055301
Menikoff R, Mjolsness R, Sharp D, Zemach C. 1977. Unstable normal mode for Rayleigh–Taylor instability in viscous fluids. *Phys. Fluids* 20:2000–2004
Mikaelian K. 1989. Turbulent mixing generated by Rayleigh-Taylor and Richtmyer-Meshkov instabilities. *Physica* 36D:343–357
Mikaelian K. 1993. Effect of viscosity on Rayleigh-Taylor and Richtmyer-Meshkov instabilities. *Phys. Rev. E* 47:375–383
Mitchner M, Landshoff R. 1964. Rayleigh-Taylor Instability for Compressible Fluids. *Phys. Fluids* 7:862–866
Mueschke N, Andrews M, Schilling O. 2006. Experimental characterization of initial conditions and spatio-temporal evolution of a small-Atwood-number Rayleigh–Taylor mixing layer. *J. Fluid Mech.* 567:27–63
Neil E, Houseman G. 1999. Rayleigh-Taylor instability of the upper mantle and its role in intraplate orogeny. *Geophys. J. Intern.* 138:89–107
Newcomb W. 1983. Compressibility effect on instability growth rates. *Phys. Fluids* 26:3246–3246
Niemela J, Skrbek L, Sreenivasan K, Donnelly R. 2000. Turbulent convection at very high Rayleigh numbers. *Nature* 404:837–840
Obukhov A. 1941. On the distribution of energy in the spectrum of turbulent flow. *C.R. Acad. Sci. URSS* 32:22–24
Obukhov A. 1949. Temperature field structure in a turbulent flow. *Izv. AN SSSR Geogr. and Geophys.* 13:58–69
Obukhov A. 1959. Effect of Archimedean forces on the structure of the temperature field in a turbulent flow. *Dokl. Akad. Nauk SSSR* 125:1246–1249
Peterson D, Bowers R, Brownell J, Greene A, McLenithan K, et al. 1996. Two-dimensional modeling of magnetically driven Rayleigh–Taylor instabilities in cylindrical Z pinches. *Phys. Plasmas* 3:368–381
Plesset M. 1954. On the Stability of Fluid Flows with Spherical Symmetry. *J. Applied Phys.* 25:96–98
Poujade O. 2006. Rayleigh-Taylor Turbulence is Nothing Like Kolmogorov Turbulence in the Self-Similar Regime. *Phys. Rev. Lett.* 97:185002
Qiu X, Liu Y, Zhou Q. 2014. Local dissipation scales in two-dimensional Rayleigh-Taylor turbulence. *Phys. Rev. E* 90:043012
Ramaprabhu P, Andrews M. 2004. Experimental investigation of Rayleigh–Taylor mixing at small Atwood numbers. *J. Fluid Mech.* 502:233–271
Read K. 1984. Experimental investigation of turbulent mixing by Rayleigh-Taylor instability. *Physica* 12D:45–58
Ristorcelli J, Clark T. 2004. Rayleigh–Taylor turbulence: self-similar analysis and direct numerical simulations. *J. Fluid Mech.* 507:213–253
Rivera M, Ecke R. 2006. The Rayleigh-Taylor instability in small aspect ratio containers. *Proc. IWPCTM10* 0:0
Sakagami H, Nishihara K. 1990. Three-dimensional Rayleigh–Taylor instability of spherical systems. *Phys. Rev. Lett.* 65:432–435

Scagliarini A, Biferale L, Sbragaglia M, Sugiyama K, Toschi F. 2010. Lattice Boltzmann methods for thermal flows: Continuum limit and applications to compressible Rayleigh–Taylor systems. *Phys. Fluids* 22:055101

Schneider M, Dimonte G, Remington B. 1998. Large and small scale structure in Rayleigh-Taylor mixing. *Phys. Rev. Lett.* 80:3507

Sharp D. 1984. An overview of Rayleigh-Taylor instability. *Physica* 12D:3–18

Shultz D, Kanak K, Straka JM, Trapp R, Gordon B, et al. 2006. The mysteries of mammatus clouds: Observations and formation mechanisms. *J. Atmos. Sci.* 63:2409–2435

Siggia E. 1994. High Rayleigh Number Convection. *Annu. Rev. Fluid Mech.* 26:137–168

Snider D, Andrews M. 1994. Rayleigh–Taylor and shear driven mixing with an unstable thermal stratification. *Phys. Fluids* 6:3324–3334

Soulard O. 2012. Implications of the Monin-Yaglom relation for Rayleigh-Taylor turbulence. *Phys. Rev. Lett.* 109:254501

Soulard O, Griffond J. 2012. Inertial-range anisotropy in Rayleigh-Taylor turbulence. *Phys. Fluids* 24:025101

Soulard O, Griffond J, Gréa B. 2015. Large-scale analysis of unconfined self-similar Rayleigh–Taylor turbulence. *Phys. Fluids* 27:095103

Spiegel E. 1971. Convection in stars: I. Basic Boussinesq convection. *Annu. Rev. Astronomy Astrophys.* 9:323

Sreenivasan K, Antonia R. 1997. The Phenomenology of small-scale turbulence. *Annu. Rev. Fluid Mech.* 29:435–472

Sreenivasan KR, Abarzhi SI. 2013. Acceleration and turbulence in rayleigh–taylor mixing. *Phil. Trans. R. Soc. Lond. A* 371:20130267

Stevens R, Verzicco R, Lohse D. 2010. Radial boundary layer structure and Nusselt number in Rayleigh–Bénard convection. *J. Fluid Mech.* 643:495–507

Sultan P. 1996. Linear theory and modeling of the Rayleigh–Taylor instability leading to the occurrence of equatorial spread F. *J. Geophys. Res.: Space Phys.* 101:26875–26891

Sureshkumar R, Beris A. 1995. Effect of artificial stress diffusivity on the stability of numerical calculations and the flow dynamics of time-dependent viscoelastic flows. *J. Non-Newtonian Fluid Mech.* 60:53–80

Tabak M, Hammer J, Glinsky M, Kruer W, Wilks S, et al. 1994. Ignition and high gain with ultrapowerful lasers. *Phys. Plasmas* 1:1626–1634

Tao J, He X, Ye W, Busse F. 2013. Nonlinear Rayleigh-Taylor instability of rotating inviscid fluids. *Phys. Rev. E* 87:013001

Tritton D. 1988. Physical fluid dynamics. Oxford Clarendon Press

Virk P. 1975. Drag reduction fundamentals. *AIChE J.* 21:625–656

Vladimirova N, Chertkov M. 2009. Self-similarity and universality in Rayleigh–Taylor, Boussinesq turbulence. *Phys. Fluids* 21:015102

Vladimirova N, Rosner R. 2003. Model flames in the Boussinesq limit: the effects of feedback. *Phys. Rev. E* 67:066305

Warhaft Z. 2000. Passive Scalars in Turbulent Flows. *Annu. Rev. Fluid Mech.* 32:203–240

Watanabe T, Gotoh T. 2004. Statistics of a passive scalar in homogeneous turbulence. *New J. Physics* 6:40

Watanabe T, Gotoh T. 2006. Intermittency in passive scalar turbulence under the uniform mean scalar gradient. *Phys. Fluids* 18:058105

Weinberg R, Schmeling H. 1992. Polydiapirs: multiwavelength gravity structures. *J. Struct. Geol.* 14:425–436

Wilson P, Andrews M. 2002. Spectral measurements of Rayleigh–Taylor mixing at small Atwood number. *Phys. Fluids* 14:938–945

Xie Y, Huang S, Funfschilling D, Li X, Ni R, Xia K. 2015. Effects of polymer additives in the bulk of turbulent thermal convection. *J. Fluid Mech.* 784:R3

Young Y, Tufo H, Dubey A, Rosner R. 2001. On the miscible Rayleigh–Taylor instability: two and three dimensions. *J. Fluid Mech.* 447:377–408

Youngs D. 1991. Three-dimensional numerical simulation of turbulent mixing by Rayleigh–Taylor instability. *Phys. Fluids A* 3:1312–1320

Youngs D. 1992. Experimental investigation of turbulent mixing by Rayleigh-Taylor instability. *in Adv. Compr. Turb. Mixing* :607–626

Zhou Q. 2013. Temporal evolution and scaling of mixing in two-dimensional Rayleigh-Taylor turbulence. *Phys. Fluids* 25:085107

Zhou Y. 2001. A scaling analysis of turbulent flows driven by Rayleigh–Taylor and Richtmyer–Meshkov instabilities. *Phys. Fluids* 13:538–543